MASTER

LBL-13486

CONF-811012--51

Lawrence Berkeley Laboratory

UNIVERSITY OF CALIFORNIA

Presented at the IEEE Nuclear Science Symposium, San Francisco, CA, October 21-23, 1981, and to be published in IEEE Transactions on Nuclear Science, NS-29(1), 1982

MONTE CARLO CALCULATIONS OF THE OPTICAL COUPLING BETWEEN BISMUTH GERMANATE CRYSTALS AND PHOTOMULTIPLIER TUBES

Stephen E. Derenzo and John K. Riles

October 1981

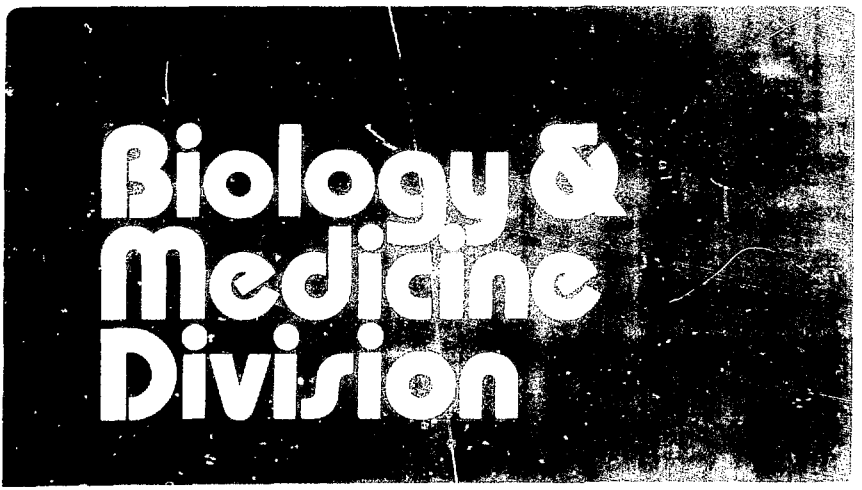

Prepared for the U.S. Department of Energy under Contract W-7405-ENG-48

DISTRIBUTION OF THIS DOCUMENT IS UNLIMITED

MONTE CARLO CALCULATIONS OF THE OPTICAL COUPLING BETWEEN BISMUTH GERMANATE CRYSTALS AND PHOTOMULTIPLIER TUBES*

Stephen E. Derenzo and John K. Riles

Donner Laboratory and Lawrence Berkeley Laboratory
University of California
Berkeley CA 94720

LBL--13486

DE82 004845

Summary

The high density and atomic number of bismuth germanate ($Bi_4Ge_3O_{12}$ or BGO) make it a very useful detector for positron emission tomography. Modern tomograph designs use large numbers of small, closely-packed crystals for high spatial resolution and high sensitivity. However, the low light output, the high refractive index (n=2.15), and the need for accurate timing make it important to optimize the transfer of light to the photomultiplier tube (PMT). We describe the results of a Monte Carlo computer program developed to study the effect of crystal shape, reflector type, and the refractive index of the PMT window on coupling efficiency. The program simulates total internal, external, and Fresnel reflection as well as internal absorption and scattering by bubbles. We show that when internal trapping in clear, polished BGO crystals is reduced by (a) suitable crystal shaping, (b) a PMT window with a high refractive index, or (c) non-absorbing vacuum bubbles, it is possible to transfer more than 60% of the scintillation light to the PMT. This transfer is greatly reduced by internal absorption.

1. Introduction

The high density and atomic number of BGO make it a very useful detector for applications such as positron emission tomography.[1] However, the low light output and the scintillation decay time of 300 nsec make the timing accuracy very dependent upon the optical coupling efficiency between the crystal and the PMT. The low light output is partly a result of the high refractive index of BGO (n=2.15) that causes trapping of light within the crystal. However, the ease of handling BGO (which is not affected by air or moisture) facilitates the use of a wide variety of crystal shapes, surface treatments (polished, rough), and external reflectors ($BaSO_4$, MgO, TiO_2, etc.)

Our objective is the design of a system with multiple rings of small closely-packed crystals coupled individually to PMTs. Therefore, most of the examples presented here are for rectangular BGO crystals with a 6.5 mm x 20 mm face partially coupled to a 14 mm diameter PMT to permit stacking in a two dimensional array.

Previous work has shown the importance of the shape of the scintillator and lightpipe for single detectors of cylindrical symmetry.[2,3,4,5] However, this work concentrates on the efficient coupling of small closely-packed arrays of rectangular BGO crystals to closely-packed cylindrical PMTs, with special attention to special crystal shapes and the effects of internal absorption and bubbles. Lightpipes were not considered in this work.

2. Computer Code

Figure 1 shows the flow chart for the Monte Carlo computer program, which runs on a Digital Equipment Corp. PDP-11/34 computer under RSX-11M. For the cases presented here, computation time varied from 0.2 to 20 sec per photon, depending on parameters.

Program input is either read from a disc file or entered interactively from the keyboard. The locations of the scintillation flashes are generated in two modes: (a) exponentially throughout the crystal to simulate broad beam exposure to 511 keV photons, and (b) on a grid of positions to determine the uniformity of light collection. The initial photon direction is randomly isotropic in both cases.

Each scintillati photon is tracked as it reflects from the surfac of the crystal and scatters on bubbles until it is ei er absorbed, collected by the PMT, or considered trapped. Internal absorption and bubble scattering occur whenever a corresponding random interaction length is ser than the next surface along the path. The bubbl scattering angle is computed from formulas for reflection from the surface of the bubble or refraction through the bubble, depending on a randomly derived impact radius.

At a polished crystal rface, the angle of incidence determines whether e photon is internally reflected. If not, a random umber determines whether the photon undergoes Fresnel reflection at that angle or exits the crystal. Depend on the surface, exited photons are either collected the PMT or reach the external reflector. In the ter case, the program compares a new random number with the reflectivity value to determine whether the photon is absorbed or redirected toward the crystal and refracted at the interface. The program assumes that there is a thin layer of air between the polished surface and the external reflector and that the angle of reflection is uniformly isotropic and independent of incident angle.

At a rough crystal surface, the photon may either be absorbed or reflected isotropically back into the crystal.

At a metalized crystal surface, the photon may either be absorbed or reflected specularly back into the crystal.

A photon is considered trapped if it has made 500 surface contacts without absorption or collection. For a polished, clear, rectangular crystal a photon is considered trapped whenever internal reflections have occurred on all surfaces. Note that the portion of the crystal in optical contact with the PMT is considered a separate surface.

To check the program and to gain a perspective on how photons are absorbed and collected for crystals of various shapes, an option was provided that displays the crystal outline and the path of each photon in a video graphics monitor.

3. Results

The program was used to simulate the six crystal shapes shown in Fig 2A-2F. The quantities tabulated by the program are defined in Table 1.

Due to limited space, we report only on the amount of light collected, which for BGO is the major factor in good timing resolution. The positional uniformity of light collection, which influences pulse height resolu-

*S nmental
Re act No.
W- tes of
He.

DISTRIBUTION OF THIS DOCUMENT IS UNLIMITED

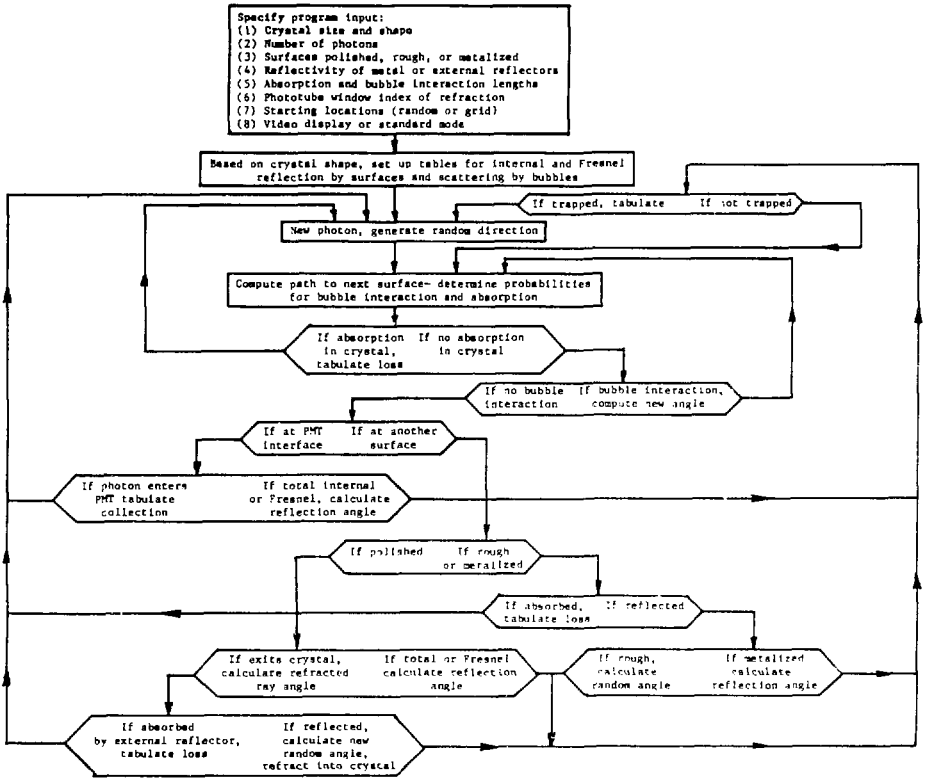

Figure 1. Flow chart of Monte Carlo computer program used in this work

tion, is of less importance for positron emission tomography. Topics such as pulse height resolution, and time of flight variations within the crystal will be treated in another report.

TABLE 1. Glossary of terms used in Tables 2-10

S: P, D, or M surface types
- P: Polished and coated with white powder
- D: Rough and coated with white powder
- M: Polished and evaporated with aluminum

R_{ext}: Reflectivity of external reflector
PMT_n: Index of refraction of PMT window
L_{int}: Mean path length for internal absorption
L_{bub}: Mean path length for scattering on vacuum bubbles
C: Percent collected by PMT
T: Percent trapped by internal reflection
A_{int}: Percent absorbed internally
A_{ext}: Percent absorbed by external reflector
L_C: Average path length for collected photons
L_{all}: Average path length for all photons
N_C: Average number of surface contacts for collected photons
N_{all}: Average number of surface contacts for all photons

Table 2 shows that when a clear, polished BGO cube is coupled to a PMT with standard index of refraction (n= 1.52), 48% of the light is trapped by total internal reflection, 23% is absorbed on the external reflector, and only 29% is collected by the PMT (line 1). When the same crystal is coupled to a PMT with n=2.0, only 16% is trapped and 7% is absorbed externally, while 77% is collected, a 2.7-fold increase (line 2).

We have measured several very clear BGO crystals with a spectrophotometer and find (after correcting for Fresnel reflection) that an attenuation length of 200mm is typical at 480 nm, the emission wavelength of BGO. This narrow beam measurement includes both absorption and scattering by bubbles. In these tables, we have chosen both the absorption length and the bubble interaction length to be 400 mm. The combined effect is consistent with our measurements.

Table 2 (lines 3 and 4) shows that absorption and bubbles eliminate trapping but result in a large percentage of internally absorbed photons. By randomizing the photon direction, scattering on bubbles aids collection while absorption reduces collection. The net effect depends on the situation. Table 2 (lines 5-8)

shows that a diffuse reflectivity also eliminates trapping and this can compensate for increased losses at the reflecting surfaces. Table 2 (lines 9-12) shows that evaporated aluminum results in a low collection, in agreement with our measurements.

Table 3 shows that only 10-20% of the collected light is lost by reducing the size of the crystal from a 30mm cube to 30mm x 20mm x 6.5mm.

Table 4 shows that when this narrow crystal is half coupled to the PMT the collection is decreased (compare with Table 3). For clear BGO with polished surfaces (lines 1-2) the loss is less than when absorption is present (lines 3-4). We have measured a 40% loss in PMT pulse height when a diffuse reflector is inserted between the crystal and the PMT to cover one half of the face.

Table 5 shows the effect of sloping the faces (Fig 2C). For clear, polished BGO the improvement is quite substantial (compare line 1 with 3 or 5 or 7, etc.), but the effect is reduced for BGO with absorption (compare line 2 with 4, 6, 8, etc.). Nonetheless, it appears possible to increase the collection from 27% (line 2) to over 40% (e.g. line 4), which is a useful gain. Unfortunately, the best gains are achieved using rather extreme shapes.

Table 6 shows that for a moderately shaped polished crystal, the collection is not a strong function of the external reflectivity (compare lines 3 and 5). For a diffuse reflector, however, good collection is only achieved when the external reflectivity is high (compare lines 8-10).

Table 7 shows that for polished crystals internal absorption has a very strong effect on the amount collected. An absorption length of 100 mm results in only 16% collection (line 1) while an absorption length of 1000 mm results in 45% collection (line 4).

Table 8 shows that a serrated end improves the light output of polished crystals (compare with Table 4, line 3). but not much more than a simple slope does (see Table 5, line 4). The same is true for the pyramidal end (Fig 2E, Table 9) and the parabolic end (Fig 2F, Table 10).

4. Conclusions

Our main conclusions are summarized below:

(1) In a clear, polished, rectangular BGO crystal about half of the light is internally trapped (Table 2, line 1). There are three ways to enable some of this trapped light to be collected: (a) use a PMT window with high index of refraction, (b) modify the shape of the crystal, and (c) disperse non-absorbing vacuum bubbles uniformly within the crystal.

(2) Suitable shaping of the crystal is the easiest way to reduce internal trapping and for clear crystals can result in a collection of over 60% of the scintillation light (Table 5, line 9).

(3) Even when internal trapping is low, a large percentage may be lost to internal absorption. In the cases examined, a photon absorption length as large as 10 times the size of the crystal reduced the collection by a factor of two (Table 7, compare lines 3 and 6).

(4) For clear crystals partial coupling to the PMT does not result in a serious loss in the collected light. The loss is greater for crystals with internal absorption. (Compare Tables 3 and 4).

(5) The use of evaporated metal as a reflector results in poorer collection than polished or diffuse surfaces. In the cases studied, the collection with polished surfaces was less sensitive to the external reflectivity than diffuse surfaces (Table 6, compare lines 1-5 with 6-10). Thus the relative merit of polished and diffuse surfaces depends on the reflectivity of the external reflector.

(6) The various shapes shown in Figs 2D-2F do not perform better than the shape in Fig 2C (compare Tables 8, 9,10 with Table 5).

Acknowledgments

We thank T.F. Budinger and R.H. Huesman for helpful discussions and T. Vuletich for technical assistance. This work was supported by the Office of Health and Environmental Research of the U.S. Department of Energy under Contract No. W-7405-ENG-48 and the U.S. National Inatitutes of Health under grant No. P01 HL25840-02.

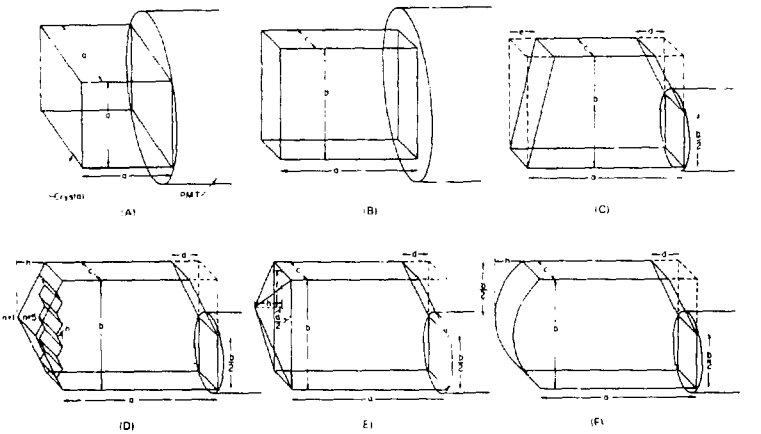

Figure 2. Crystal shapes considered

UBL8110-4292

REFERENCES

1. Derenzo SE, Budinger TF, Huesman, RH, et al: Imaging properties of a positron tomograph with 280 BGO crystals. IEEE Trans Nucl Sci NS-28: No 1, 81-89, 1981

2. Falk F and Sparrman P: A computer method for the evaluation of the optical properties of scintillation detector assemblies. Nucl Instr Math 85: 253-258, 1970

3. Klein H and Schöllermann H: Improvement of the light collection in scintillation detectors. IEEE Trans Nucl Sci NS-26: No 1, 373-377, 1979

4. Schöllermann H and Klein H: Optimizing the energy resolution of scintillation counters at high energies. Nucl Instr Meth 169: 25-31, 1980

5. Neiler JH and Bell PR: The scintillation method. In Alpha-, Beta- and Gamma-ray Spectroscopy (Siegbahn K, Ed), North-Holland, Amsterdam, 1965

TABLE 2. Collection and Loss for a Fully Coupled BGO Cube (Fig 2A)
(a=30mm, 10,000 photons each)

Line No.	S	R_{ext} (%)	PMT_n	L_{int} (mm)	L_{bub} (mm)	C (%)	T (%)	A_{int} (%)	A_{ext} (%)	L_C (mm)	L_{all} (mm)	N_C	N_{all}
1	P	98	1.52	∞	∞	29	48	0	23	40	∞	2.5	∞
2	P	98	2.00	∞	∞	77	16	0	7	156	∞	7.9	∞
3	P	98	1.52	400	400	36	0	62	3	132	248	7.0	12.6
4	P	98	2.00	400	400	66	0	32	2	95	123	5.1	6.5
5	D	98	1.52	∞	∞	85	0	0	15	151	149	9.1	9.0
6	D	98	2.00	∞	∞	89	0	0	11	106	103	6.4	6.3
7	D	98	1.52	400	400	60	0	29	11	117	114	7.1	7.1
8	D	98	2.00	400	400	70	0	21	9	91	86	5.6	5.4
9	M	90	1.52	∞	∞	25	0	0	75	38	165	2.3	8.7
10	M	90	2.00	∞	∞	52	0	0	48	45	104	2.8	5.5
11	M	90	1.52	400	400	26	0	27	47	59	108	3.3	5.8
12	M	90	2.00	400	400	48	0	18	34	57	74	3.3	4.1

TABLE 3. Collection and Loss for a Fully Coupled Narrow Rectangular BGO Crystal (Fig 2B)
(a=30mm, b=20 mm, c=6.5 mm, 10,000 photons each)

Line No.	S	R_{ext} (%)	PMT_n	L_{int} (mm)	L_{bub} (mm)	C (%)	T (%)	A_{int} (%)	A_{ext} (%)	L_C (mm)	L_{all} (mm)	N_C	N_{all}
1	P	98	1.52	∞	∞	30	47	0	23	42	∞	4.5	∞
2	P	98	2.00	∞	∞	70	16	0	14	110	∞	12.4	∞
3	P	98	1.52	400	400	34	0	59	6	174	238	14.6	28.7
4	P	98	2.00	400	400	65	0	30	6	81	121	11.4	15.7
5	D	98	1.52	∞	∞	70	0	0	30	133	128	16.3	16.1
6	D	98	2.00	∞	∞	74	0	0	26	112	108	13.8	13.6
7	D	98	1.52	400	400	51	0	25	24	107	99	13.0	12.7
8	D	98	2.00	400	400	57	0	22	21	97	90	11.8	11.5
9	M	90	1.52	∞	∞	22	0	0	78	36	69	3.8	8.5
10	M	90	2.00	∞	∞	39	0	0	61	41	51	4.8	6.4
11	M	90	1.52	400	400	20	0	15	65	40	58	4.1	7.2
12	M	90	2.00	400	400	37	0	11	52	44	44	5.1	5.7

TABLE 4. Collection and Loss for a Half Coupled Narrow Rectangular BGO Crystal (Fig 2C)
(a=30 mm, b=20 mm, c=6.5 mm, d=0mm, e=0mm, 10,000 photons each)

Line No.	S	R_{ext} (%)	PMT_n	L_{int} (mm)	L_{bub} (mm)	C (%)	T (%)	A_{int} (%)	A_{ext} (%)	L_C (mm)	L_{all} (mm)	N_C	N_{all}
1	P	98	1.52	∞	∞	28	49	0	23	141	∞	14.1	∞
2	P	98	2.00	∞	∞	66	17	0	17	224	∞	25.4	∞
3	P	98	1.52	400	400	26	0	67	7	173	270	19.6	32.3
4	P	98	2.00	400	400	51	0	43	6	146	170	17.1	20.9
5	D	98	1.52	∞	∞	53	0	0	47	199	192	24.6	24.2
6	D	98	2.00	∞	∞	59	0	0	41	172	164	21.4	20.7
7	D	98	1.52	400	400	34	0	34	32	143	130	17.7	16.8
8	D	98	2.00	400	400	40	0	30	30	128	119	15.8	15.3
9	M	90	1.52	∞	∞	15	0	0	85	61	74	5.7	8.9
10	M	90	2.00	∞	∞	25	0	0	75	60	64	6.3	7.7
11	M	90	1.52	400	400	12	0	16	72	56	63	5.4	7.6
12	M	90	2.00	400	400	21	0	14	65	59	56	6.3	6.9

TABLE 5. Collection and Loss for a Half Coupled Narrow BGO Crystal with Sloped Faces (Fig 2C)
(a=30 mm, b=20 mm, c=6.5 mm, R_{ext}=98%, PMT_n=1.52, S=P, 10,000 photons each)

Line No.	d (mm)	e (mm)	L_{int} (mm)	L_{bub} (mm)	C (%)	T (%)	A_{int} (%)	A_{ext} (%)	L_C (mm)	L_{all} (mm)	N_C	N_{all}
1	0.0	0.0	∞	∞	29	49	0	22	143	∞	14.2	∞
2	0.0	0.0	400	400	27	0	66	7	170	275	19.3	32.8
3	0.0	10.0	∞	∞	61	22	0	17	423	∞	50.5	∞
4	0.0	10.0	400	400	35	0	59	6	180	240	21.4	30.1
5	0.0	20.0	∞	∞	57	28	0	15	195	∞	23.8	∞
6	0.0	20.0	400	400	42	0	52	6	156	209	20.2	28.5
7	10.0	0.0	∞	∞	55	28	0	17	375	∞	39.8	∞
8	10.0	0.0	400	400	30	0	63	6	196	254	22.1	30.9
9	10.0	10.0	∞	∞	64	20	0	16	411	∞	51.0	∞
10	10.0	10.0	400	400	36	0	58	7	177	233	21.4	29.7
11	10.0	20.0	∞	∞	58	27	0	15	159	∞	20.1	∞
12	10.0	20.0	400	400	44	0	50	7	147	194	19.7	27.3
13	20.0	0.0	∞	∞	57	25	0	18	435	∞	51.3	∞
14	20.0	0.0	400	400	31	0	61	7	197	249	23.2	31.1
15	20.0	10.0	∞	∞	65	20	0	15	330	∞	42.7	∞
16	20.0	10.0	400	400	39	0	54	7	173	216	21.9	28.9
17	20.0	20.0	∞	∞	65	22	0	14	227	∞	32.7	∞
18	20.0	20.0	400	400	47	0	47	6	138	187	19.2	27.0

TABLE 6. Collection and Loss for a Half Coupled, Narrow, Sloped BGO Crystal with Various External Reflectivities (Fig 2C)
(a=30 mm, b=20 mm, c=6.5 mm, d=0 mm, e=10 mm, L_{int}=L_{bub}=400mm, PMT_n=1.52, S=P, 10,000 photons)

Line No.	S	R_{ext} (%)	C (%)	T (%)	A_{int} (%)	A_{ext} (%)	L_C (mm)	L_{all} (mm)	N_C	N_{all}
1	P	0	20	0	35	45	145	141	19.0	18.7
2	P	50	25	0	40	35	152	162	19.3	21.0
3	P	90	32	0	51	18	165	202	19.8	25.1
4	P	98	34	0	60	7	195	244	23.0	30.4
5	P	100	36	0	64	0	198	259	23.3	32.3
6	D	0	2	0	1	97	14	6	1.0	1.0
7	D	50	4	0	4	93	23	13	2.2	1.9
8	D	90	17	0	14	70	63	53	7.6	7.2
9	D	98	38	0	30	31	130	121	16.9	16.3
10	D	100	56	0	44	0	178	173	23.7	23.5

TABLE 7. Collection and Loss for a Half Coupled, Narrow, Sloped, BGO Crystal with Various Internal Absorption Lengths (Fig 2C)
(a=30mm, b=20mm, c=6.5mm, d=0mm, e=10mm, R_{ext}=98%, PMT_n=1.52, S=P, 10,000 photons each)

Line No.	L_{int} (mm)	L_{bub} (mm)	C (%)	T (%)	A_{int} (%)	A_{ext} (%)	L_C (mm)	L_{all} (mm)	N_C	N_{all}
1	100	∞	16	0	81	3	69	81	7.9	11.4
2	200	∞	24	0	70	6	110	141	12.4	19.2
3	400	∞	34	0	58	8	152	229	17.1	31.4
4	1000	∞	46	0	42	11	242	426	27.8	59.4
5	2000	∞	52	0	35	14	323	686	38.0	98.4
6	∞	∞	62	22	0	16	425	∞	50.6	∞

TABLE 8. Collection and Loss for a Half Coupled, Narrow, BGO Crystal with Serrated End (Fig 2D)
(a=30mm, b=20mm, c=6.5mm, d=0mm, R_{ext}= 98%, S= P, R_{ext}=98%, L_{int}=L_{bub}=400mm, PMT_n=1.52, 10,000 photons each)

Line No.	n	h (mm)	C (%)	T (%)	A_{int} (%)	A_{ext} (%)	L_C (mm)	L_{all} (mm)	N_C	N_{all}
1	1	5.00	34	0	60	6	201	241	22.1	28.6
2	2	2.50	35	0	59	6	191	237	21.3	28.5
3	3	1.67	34	0	59	6	186	237	20.9	28.6
4	4	1.25	34	0	59	6	190	235	21.2	28.3
5	5	1.00	35	0	58	6	180	232	20.4	28.1

TABLE 9. Collection and Loss for a Half Coupled, Narrow BGO Crystal with Pyramidal End (Fig 2E)
(a=30 mm, b=20 mm, c=6.5 mm, d=0 mm, R_{ext}=98%, PMT_n=1.52, S=P, L_{int}=L_{bub}=400 mm, 10,000 photons each)

Line No.	f (mm)	h (mm)	C (%)	T (%)	A_{int} (%)	A_{ext} (%)	L_C (mm)	L_{all} (mm)	N_C	N_{all}
1	0.0	0	27	0	66	7	170	275	19.3	32.8
2	3.3	2	35	0	59	6	192	236	22.1	26.8
3	6.7	2	36	0	59	5	194	231	22.1	26.3
4	10.0	2	36	0	58	6	193	231	22.2	26.3
5	3.3	4	37	0	57	6	190	227	21.4	25.9
6	6.7	4	37	0	58	5	190	227	21.5	25.9
7	10.0	4	36	0	58	6	192	234	21.6	26.8
8	3.3	6	38	0	57	5	184	223	20.6	25.6
9	6.7	6	38	0	57	5	194	227	21.6	26.1
10	10.0	6	38	0	58	5	190	228	21.1	26.2

TABLE 10. Collection and Loss for a Half Coupled, Narrow, BGO Crystal with a Parabolic End (Fig 2F)
(a=30mm, b=20mm, c=6.5mm, R_{ext}=98%, PMT_n=1.52, L_{int}=L_{bub}=400mm, S=P, 10,000 photons each)

Line No	d (mm)	h (mm)	C (%)	T (%)	A_{int} (%)	A_{ext} (%)	L_C (mm)	L_{all} (mm)	N_C	N_{all}
1	0.0	2	32	0	61	7	197	241	21.7	28.9
2	10.0	2	36	0	57	6	196	230	22.2	28.0
3	0.0	4	33	0	60	6	193	238	20.9	28.2